Iraqi Journal of Physics, 2025 *Vol.23, No.2, PP.1-12*
https://doi.org/10.30723/ijp.v23i2.1467
P-ISSN: 2070-4003
E-ISSN: 2664-5548

Contribution to the Development of Nano-Composite Materials Based on ZnO and Polymethyl Methacrylate Structural and Optical Study

Abdellah Elkaiem[1*] and Omar Boukraa[1]
[1]*University of Ouargla, Faculty of Mathematics and Material Sciences, Laboratory for the Development of New and Renewable Energies in Arid and Saharan Zones, Ouargla 30000, Algeria*
*Corresponding author: kaim.a.allah@gmail.com

Abstract

In this study, thin films of pure and aluminum (Al)-doped zinc oxide/polymethyl methacrylate (ZnO/PMMA) with two different amounts (5% and 7%) using the sol-gel and spin coating methods were created and then heated at two temperatures (450 and 750°C). Many characteristics were used to analyze the resulting samples, including X-ray diffraction (XRD), UV-visible, and infrared (IR) absorption spectroscopy. The X-ray diffraction analysis of the samples indicated that they formed a hexagonal structure of ZnO known as wurtzite, with a preferred direction labelled as (101). UV-visible analysis of the specimens' optical characteristics has helped calculate the gap energy using the Tauc method. The energy value is 4.12 eV. The optical characteristics of the samples were analyzed by the Fourier Transform Infrared (FTIR), which shows the presence of absorption peaks attributed to the existence of the new phase that cannot be observed through the X-rays, which is a phase of spinel zinc aluminate ($ZnAl_2O_4$).

Article Info.

Keywords:
Nanopowder, Thin Films of ZnO, Sol-Gel, Phase Spinel, $ZnAl_2O_4$.

Article history:
Received: Apr. 05,2025
Revised: Apr. 12, 2025
Accepted: May 27,2025
Published:Jun. 01,2025

1. Introduction

For many years, zinc oxide (ZnO) has been used mainly in the chemical and pharmaceutical industries. New avenues of research in optoelectronics, microelectronics, and spintronics are generating considerable interest in this material due to its multiple properties: high thermal conductivity, high heat capacity, medium dielectric constant, high resistivity, low water absorption, etc. ZnO was first studied in the 1970s before being abandoned by microelectronics due to the various inconclusive challenges in producing p-type ZnO. The study of this material has reemerged in the last twenty years due to its attractive fundamental properties. Technical advances in the synthesis and epitaxy of thin films, and initial results indicating the possibility of converting the conductivity of this semiconductor from n-type to p-type.

Over the past twenty years, zinc oxide thin films have gained increasing interest in numerous research projects due to their multiple potential applications. ZnO is a binary material of type II-VI, non-toxic compared to CdS, a semiconductor, photoconductor, and piezoelectric, and it can be used as an optical waveguide. It is a crystal with a hexagonal structure of the Wurtzite type. It has a large band gap of about 3.3 eV and is characterized by a transmission coefficient of about 90% in the visible spectrum. In addition, ZnO films have shown good chemical stability against hydrogen plasma, which is important in fabricating Si-H-based solar cells. ZnO thin films can be used as optical windows as well as electrodes for solar cells, in addition to their use in varistors [1] and gas sensors. Many deposition techniques have been used for the fabrication of ZnO thin films, such as laser ablation [2], RF magnetron sputtering [3], vapour deposition [4], spray pyrolysis [5] and sol-gel process [6], etc.

Doping ZnO with appropriate elements can improve its optical characteristics and accelerate the race for its practical applications. In particular, doping ZnO with aluminium significantly modifies its physical properties. ZnO nanocrystals have received specific interest due to their distinguished performances in electronics, optics and photonics. What characterizes the ZnO semiconductor is mainly its wide band gap (3.37 eV) and its high exciton binding energy (60 meV) at room temperature. The physical properties of nanocrystals depend on the size and morphology. ZnO has been developed in different morphologies such as nanowires, nanoneedles, nanotips, and nanorods [7,8]. Polymethyl methacrylate (PMMA) is one of the most important polymers derived from acrylic acid, whose optical transparency is superior to ordinary glass. In this work, undoped and Al-doped ZnO/PMMA thin films were prepared using the sol-gel technique and the spin coating technique on glass substrates.

2. Experimental Work

The sol-gel method prepared the ZnO nanofilms for their ease of use and low cost. The thin films are synthesised by spin-coating. [9] The ZnO powders and thin films were prepared on a glass substrate using pure and aluminium-doped ZnO [10]. This section will briefly describe the preparation techniques for ZnO powders and thin films.

2.1. Description of the Products and Precursors Used

The thin films are made from a mixture of PMMA [10] dissolved in tetrahydrofuran (THF) and ZnO powder. Forming and depositing the dry PMMA/THF mixture is easy, and it has excellent resistance to ageing, UV and relative surface rigidity [11,12].

2.2. Preparation of Pure ZnO Nanopowders

43.9g of zinc acetate hydrate is dissolved in 240 mL of distilled water. The resulting solution is brought to 80°C under magnetic stirring until it is clear and homogeneous.
A second solution is prepared by dissolving 2g of citric acid in 220 mL of ethanol under magnetic stirring until a clear and homogeneous solution is obtained. Using a pipette, the second solution is mixed drop by drop with the first under magnetic stirring. A white precipitate will appear, which will form the gel. The latter is left in the open air for about ten days to obtain a white powder. This white powder of pure ZnO is ground and annealed at 450°C and 750°C for one hour in an oven to get a nanometric powder of pure ZnO.

2.3 Preparation of Al-doped ZnO Nanopowders

Mixed quantities of commercial 50nm ZnO powder and pure white ZnO powder were used to obtain aluminium-doped ZnO nanopowders. To obtain atomic doping rates of 5%, 7% of the mass of gel is mixed with a mass of alumina to get the desired Al/Zn ratio. The resulting mixture is annealed at 450 and 750°C for 1 h. In this case, annealing serves for crystallization and doping.

2.4 Preparation of Al-doped ZnO Thin Films with PMMA

For the study of optical characterizations, we developed thin films using the following method:
0.4g of PMMA is dissolved in 20 ml of THF. The resulting solution is brought to 80°C under thermal stirring and divided into five parts to obtain five solutions: A1, A2, A3, A4, and A5. Dissolving 0.08g of ZnO (5% Al-doped at 750°C/1h) in 4 ml of A1 solution produces a clear and homogeneous solution.
For the same conditions:
Dissolution of 0.04g of ZnO (7% Al doped at 750°C/1h) in 2 mL of solution A2
Dissolution of 0.04g of pure ZnO (at 450°C/1h) in 2 mL of solution A3
Dissolution of 0.04g of pure ZnO (at 750°C/1h) in 2 mL of solution A4

This solution is deposited on glass using the spin-coating method to obtain thin ZnO layers.

3. Results and Discussion

This section presents the results of characterizing pure and aluminium-doped ZnO nanopowders prepared by the sol-gel process using X-ray diffraction. The structural properties of these ZnO powders were determined. The optical properties were studied using UV-Visible and infrared absorption on thin layers of Zn powder deposited by spin-coating using PMMA as a matrix.

3.1 Characterization of the Structural Properties of Pure ZnO Nanopowders by X-ray Diffraction

Several parameters can influence the preparation of pure ZnO nanopowders by the sol-gel process: precursor concentration, temperature, and calcination time. Our objective is to determine the optimal conditions for developing nanopowders that meet our objective (good optical behaviour and a fairly fine grain size). X-ray diffraction experiments provide a list of peaks; Each peak corresponds to a family of reticular planes of index (hkl) according to the Bragg diffraction conditions. The material was identified by comparison with existing databases in the form of JCPDS files.

3.1.1 Effect of Annealing Temperature on the Structure of ZnO Nanopowders

Figs.1 and 2 represent the XRD spectra for powders synthesized at 450°C and 750°C for 1 h each, respectively.

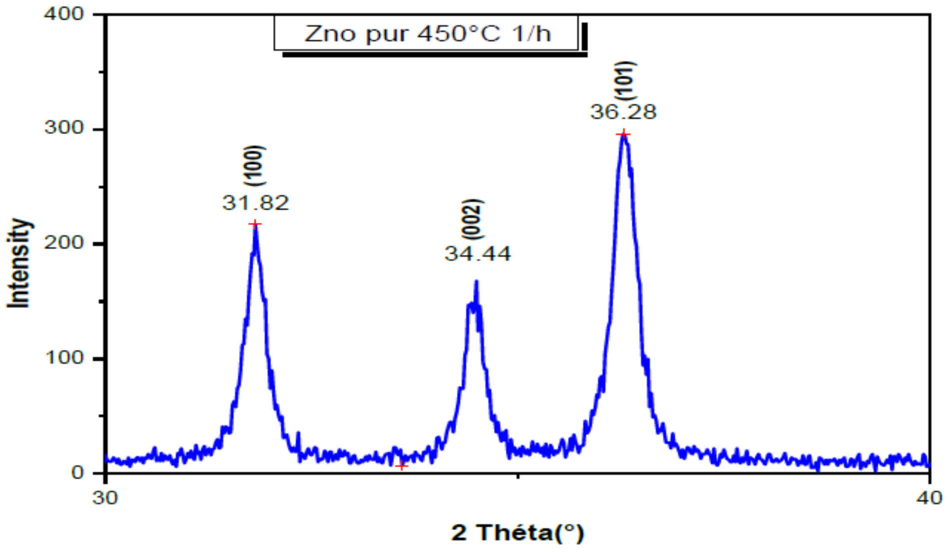

Figure 1: The X-ray diffraction spectra for powders synthesized at 450°C for 1 h.

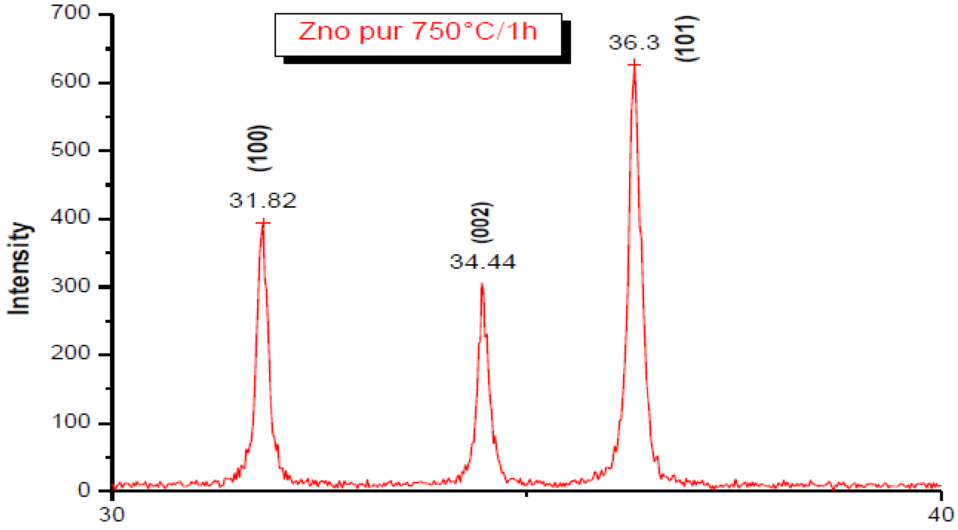

Figure 2: The X-ray diffraction spectra for powders synthesized at 750°C for 1 h.

3.1.2 Comparison between the Parameters of Pure ZnO Nanopowders of our Powders with the ASTM Data Sheet

We have summarized the results of the XRD spectra of the pure ZnO previously synthesized at (450°C, 750°C) for 1 h in the following two Tables 1 and 2, in which we compare the yields of our powders with those given in the ASTM ZnO data sheet (361451), show that:

The disappearance of certain orientations corresponding to the following planes: (110), (103), (112) in the case of 750°C firing. Our powders' yields differ slightly from those in the ASTM data sheet. This confirms the hexagonal, Würtzite-type structure of the synthesised ZnO powder. The average relative error is around 0.001. We note that the c/a ratio does not depend on the calcination temperature, at ±0.01. Using the most intense peaks (100), (002) and (101), the calculation of the parameters a and c gave average values of a = 3.24 and c = 5.19, respectively.

Table 1: Parameters of pure ZnO nano powder at 450°.

a=3.244, c=5.183 [13,14], c/a=1.59					**Reference (JCPDS)** **the ASTM data sheet for ZnO N^0 (36-1451)** a=3.249, c=5.206, c/a=1.60
Pics	**(hkl)**	**d(nm)**	**2θ(deg)**	**sinθ (deg)**	**d(nm)**
1	100	2.8091	31.82	0.274	2.816
2	002	2.5917	34.57	0.297	2.602
3	101	2.4734	36.28	0.311	2.476

Table 2: Parameters of pure ZnO nano powder at 750°C.

a=3.243, c=5.203 [13,14], c/a=1.60					**Reference (JCPDS)** **the ASTM data sheet for ZnO N^0 (36-1451)** a=3.249, c=5.206, c/a=1.60
Pics	**(hkl)**	**d(nm)**	**2θ(deg)**	**sin θ (deg)**	**d(nm)**
1	100	2.8091	31.82	0.2741	2.816
2	002	2.6013	34.44	0.296	2.602
3	101	2.4719	36.3	0.3115	2.476

3.1.3 Determination of the Grain Size of the Crystallite Size of Pure ZnO Nanopowders

From the experimental part, the grain size of our powders was determined using the following Scherrer relation [15]

$$G = \frac{0.9\lambda}{\beta \mathrm{COS}\theta} \qquad (1)$$

where: G represents the diameter of the grains assumed to be spherical, λ is the wavelength of the beam used, θ is the angular position of the line, and β is the width at half-maximum expressed in radians.

For the different powders studied, we determined the grain size using the full width at half maximum taken from the XRD spectra and by using the Debye–Scherrer formula. The results are summarized in Table 3. It is observed that the size of the crystallites increases as the calcination temperature increases. It goes from 24.59 nm for T = 450 °C to 41.81 nm for T = 750 °C. When the temperature increases from 450 to 750 °C, the width at half-height and the size of the grains varies in opposite directions.

Table 3: Effects of the calcination temperature on the tail of grains and the large size of the surface.

Calcination Temperature	**Grain size D(nm) (101)**	**width at half height FWHM(rad) (101)**
450	24.59	0.005931
750	41.81[14]	0.003488

3.2 Structural Characterization of Al-Doped ZnO Nanopowders (5%, 7%)

3.2.1 Effect of Aluminum Doping on the Nanocrystalline Structure of ZnO

Figs. 3 and 4 represent the X-ray diffraction spectra for powders synthesized at 450°C for 1 hour, and 750°C for 1 hour, respectively. In reality, doping creates constraints, which affect the intensity of the peaks. Doping shifts the angular position of the lines towards small angles. This increases the values for the (100) and (101) type lines. This shows that the parameters a have increased with doping. The counteracting effect for the (002) type lines decrease c. Note that doping does not reveal a new phase of the X-ray diffraction lines. Indeed, the peak positions correspond to hexagonal wurtzite ZnO. For example, the peaks (100), (002) and (101) are located at 2θ = 31.82°, 34.44° and 36.30 °, respectively.

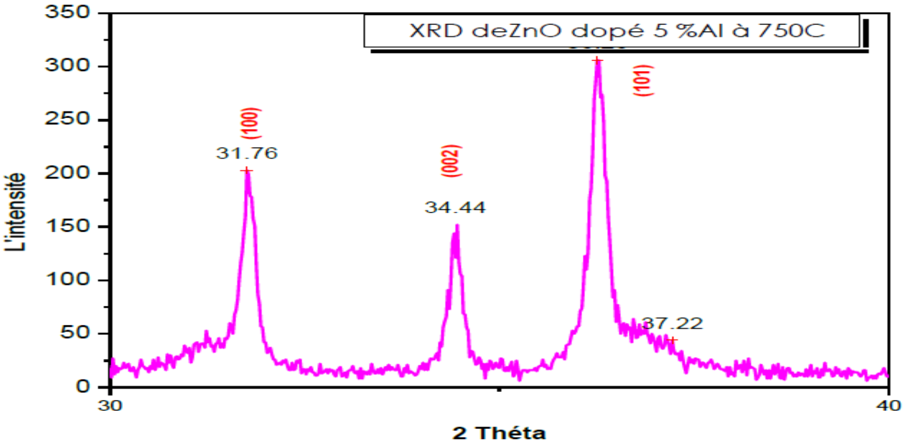

Figure 3: The X-ray diffraction spectra of Al-doped ZnO 5% at 750 °C.

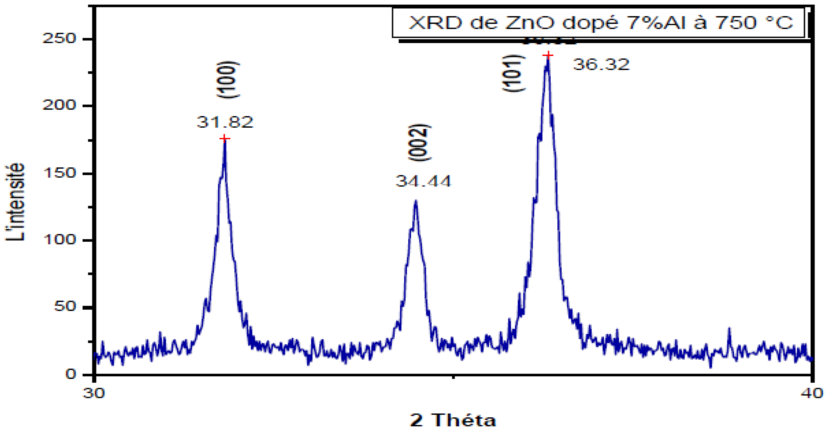

Figure 4: The X-ray diffraction spectra of Al-doped ZnO 7% at 750 °C.

3.2.2 Comparison between the Parameters of Al-Doped ZnO Nanopowders with the ASTM Data Sheet of ZnO

We have summarized the results of the previous X-ray diffraction spectra of Al-doped ZnO (5% and 7%) at 750 °C for 1 h in the following two Tables 4 and 5.

Table 4: Parameters of 5% Al doped ZnO nanopowder at 750°C/1 h.

a=3.029, c=5.247 [16] c/a=1.73					**Reference (JCPDS) the ASTM data sheet for ZnO N^0 (36-1451)** a=3.249, c=5.206, c/a=1.60
Pics	**(hkl)**	**d(nm)**	**2θ(deg)**	**in θ (deg)**	**d(nm)**
1	100	2.8143	31.76	0.2736	2.816
2	002	2.5830	34.69	0.2981	2.602
3	101	2.4750	36.26	0.3111	2.476

Table 5: Parameters of 7% Al doped ZnO nanopowder at 750°C/1 h.

a=3.244, c=5.168 [16] c/a=1.59					**Reference (JCPDS) the ASTM data sheet for ZnO N^0 (36-1451)** a=3.249, c=5.206, c/a=1.60
Pics	**(hkl)**	**d(nm)**	**2θ(deg)**	**sin θ (deg)**	**d (nm)**
1	100	2.8091	31.82	0.274	2.816
2	002	2.5838	34.68	0.298	2.602
3	101	2.4711	36.32	0.311	2.476

Tables 4 and 5 show that the values of the samples from our powders are close to those given by the ASTM data sheet. The maximum relative deviation is of the order of 0.01 and is relative to the first three most intense peaks. This deviation is probably due to the existing expansion constraints that deform the elementary mesh.

Doping creates constraints in the crystal. These constraints influence the positions of the diffraction patterns, thus creating slight variations in the inter-reticular distances and the intensity of the diffraction peaks. They also influence the a and c parameters of this hexagonal structure.

3.2.3 Effect of Doping on ZnO Grain Size

The crystal size was calculated from the width of the diffraction line at half maximum intensity in radians, obtained from XRD spectra, using the previous Debye-Scherrer formula. Table 6 shows that grain size decreases with increasing doping, ranging from 41.81 nm for pure powders to 33.44 and 22.59 nm for powders doped with 5 and 7% aluminium, respectively.

Table 6: Grain size and width at half maximum for pure and 5 and 7% Aluminum-doped ZnO powders.

Doping rate of Al% in ZnO at 750°C/1h	**Pure ZnO at 750°C/1h**	**5%**	**7%**
Grain size D(nm) (101)	41.81[14].	33.44	22.59
The width at half height FWHM(101)	0.003488	0.004361	0.0049434

3. 3 Optical Gap Study of ZnO Films

To calculate the optical gap, we used the model proposed by Tauc, where E_g is related to the absorption coefficient from the transmittance and absorption curves. By estimating the thickness of our layers, we derived the absorption coefficient α using the well-known Beer's law. In the region of strong absorption, the following relationship exists between α and hυ

$$(\alpha\, h\upsilon)=A(h\upsilon - E_g) \qquad \textbf{(2)}$$

where A is a constant related to the disorder of the structure, and E_g represents the energy gap in eV, and hυ is the photon energy in eV, and n is equal to 2 for our case, where the gap is direct.

We plotted (αhυ)^2 as a function of hυ. The value of the gap is obtained by extrapolating the linear part of the curve onto the abscissa axis (hυ) [17,18], see Figs. 5, 6, 7 below.

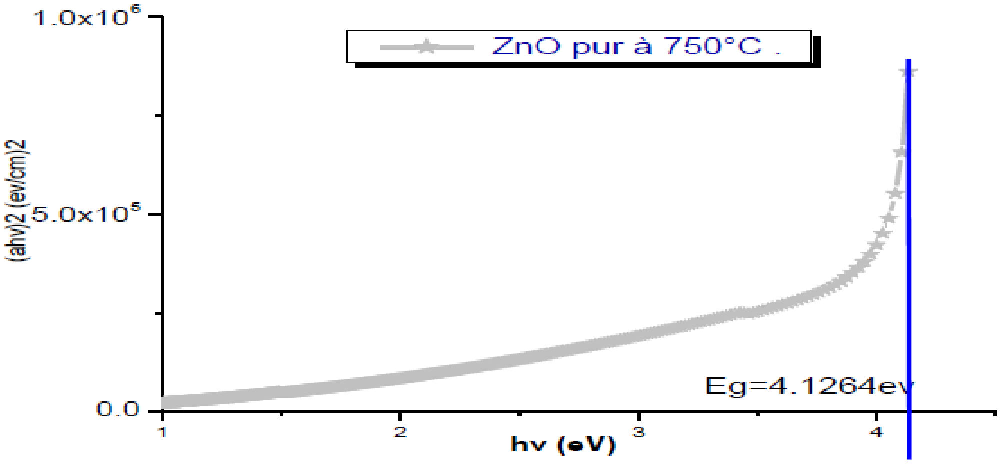

Figure 5: Tauc plot of pur ZnO thin films at 750 °C.

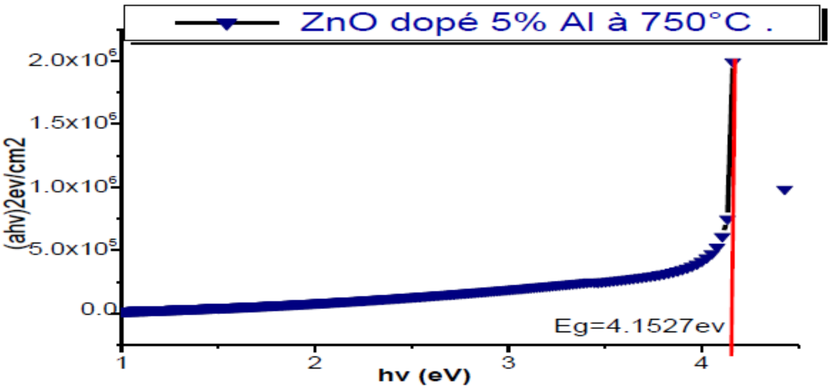

Figure 6: Tauc plot of Al-doped ZnO thin films 5% at 750 °C.

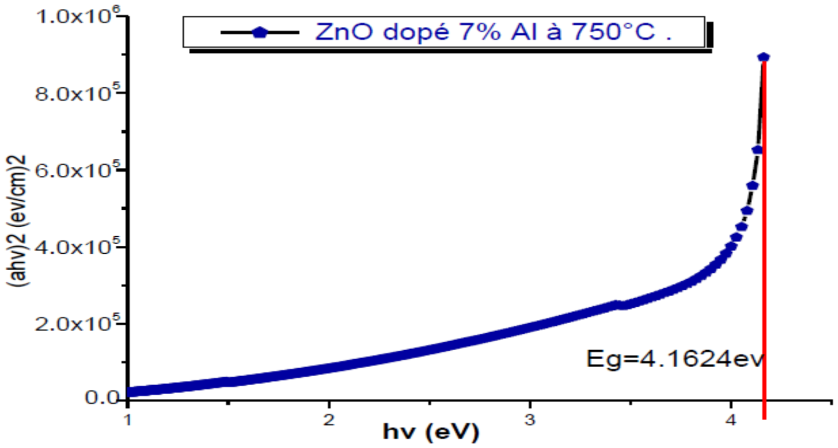

Figure 7: Tauc plot of Al-doped ZnO thin films 7% at 750 °C.

Fig.7 shows the variation of the plot of $(\alpha h\upsilon)^2$ as a function of the energy hυ for Al-doped ZnO thin films with different concentrations. We note that the band gap energy (E_g=4.12eV) increases with adding of the Al dopant [19]. This shift is due to the increase in the concentration of free carriers in the material that block the lowest states in the conduction band This increase in the gap reflects the Burstein-Moss effect, the charge carriers introduced by doping and which are released following the ionization of the donors fill the energy bands of the ZnO layers located just above the conduction band, thus causing a widening of the band gap. This phenomenon has already been observed before by other researchers. However, they disagree with those reported by other researchers who noticed that the gap energy decreases with increasing Al concentration. They attributed this decrease to the appearance of electronic defects in the band gap[20].

3.4 Study of the Refractive Index

The refractive index of each thin layer of Al-doped ZnO is determined using interference fringes (Swanepoel and Manifacier) [21,22] and transmission spectra according to the following formulas:

The thickness of the layer is determined from the following relationship

$$d = \frac{\lambda_1 \lambda_2}{2(\lambda_1 n_2 - \lambda_2 n_1)} \qquad (3)$$

The refractive indices n_1 and n_2 of the layer for wavelengths λ_1 and λ_2 are taken from the relation

$$n_{1.2} = \sqrt{N_{1.2} + \sqrt{N_{1.2}^2 + S^2}} \qquad (4)$$

S: refractive index of the substrate (=1.54) and $N_{1.2}$ can be calculated using the relation [20]

$$N_{1.2} = \left[\frac{1+S^2}{2}\right] + (2S).\left[\frac{T_{max} - T_{min}}{T_{max} T_{;in}}\right] \qquad (5)$$

The results obtained are represented in table 6 below

Table 6: The refractive index parameters.

Al's Doping	T_{max}	T_{min}	λ_1	λ_2	n1	n2	d
0%	1.272	1.11	828	832	2.134	2.145	3E5
5%	1.287	1.19	828	832	2.071	2.083	3E5
7%	1.301	1.15	828	832	2.122	2.134	3E5

It can be noted that the value of the refractive index is of the order of 2.14. Also, the refractive index can be determined using the following formula

$$n^2 = \frac{3}{\sqrt{\frac{E_g}{20}}} - 2 \tag{6}$$

where n is the refractive index of the layer to be analyzed and E_g its optical gap, the results obtained are represented in table 7 below

Table: 7: Refractive index of doped and undoped ZnO thin films.

Al's Doping	E_g	n
0	4.1264	2.1458
5	4.1527	2.1409
7	4.1624	2.1391

From the determination of the refractive index, we observe that the almost constant refractive index is of the order of 2.14.

3.5 Analysis of Infrared Spectra (FTIR) of ZnO Powders

Figs. 8, 9, 10 represent the infrareds absorption spectrum of Al-doped ZnO (0%, 5%, 7%) at 750°C/1h.

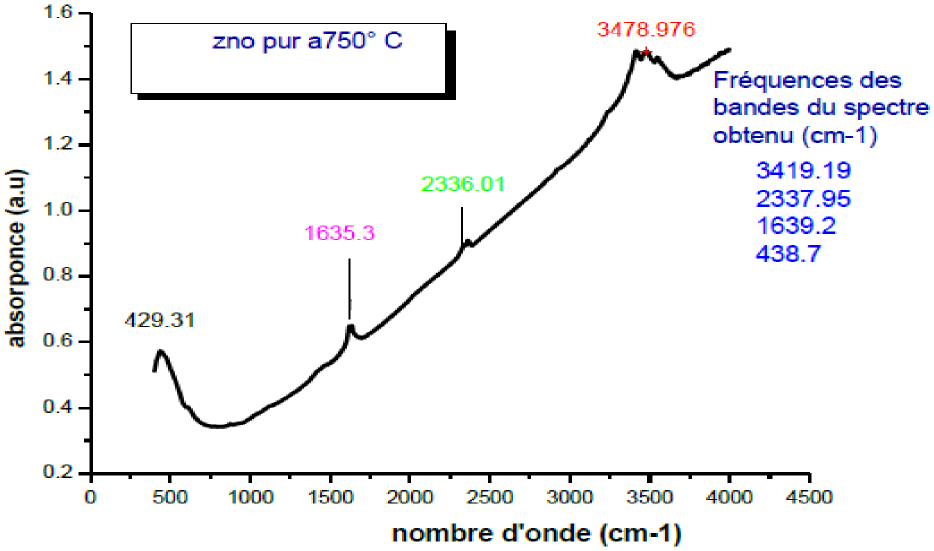

Figure 8: The Infrared spectrum of pure ZnO at T = 750°C/1 h.

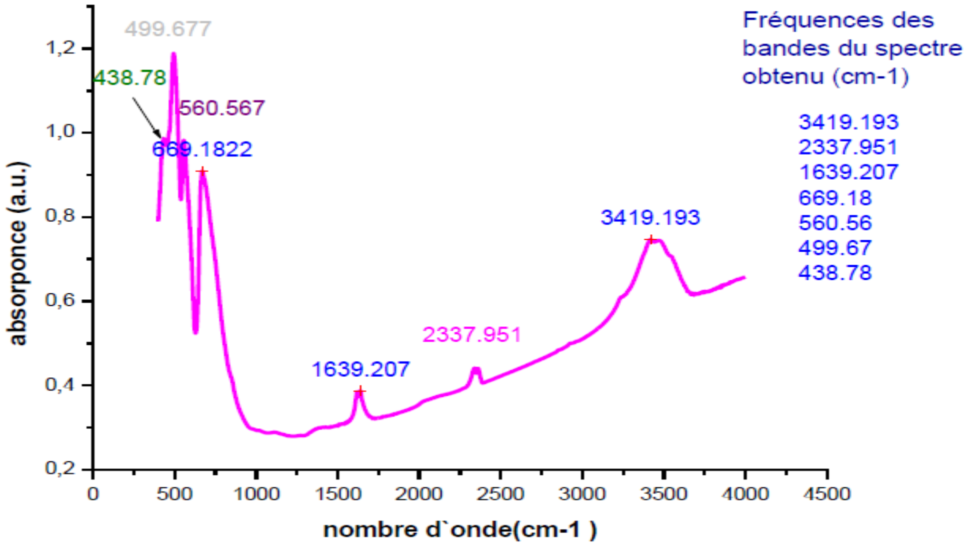

Figure 9: The Infrared spectrum of Al-doped ZnO (5% at 750 °C/1h).

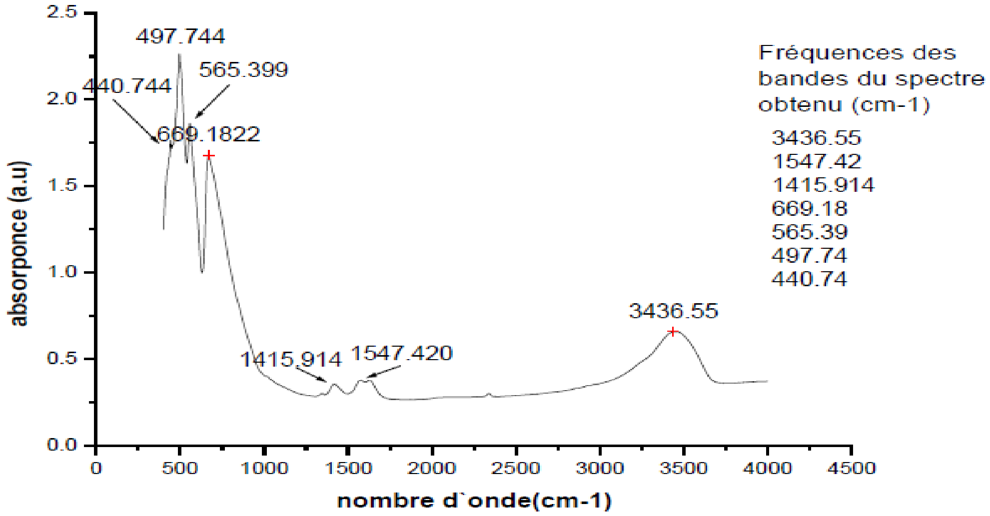

Figure 10: The Infrared spectrum of Al-doped ZnO (7% at 750 °C/1h).

From the first figure, we observe the following: An absorption band with an interface at 429.123.

After 750, there is a strong absorption with peaks appearing at 1635.3 and another at 2356.31. These peaks can be attributed to the vibration frequency of the C=O bond, compared to the value of 2359, which is the value of C=O in carbon dioxide present in air. At 3478.9, a broad, asymmetric absorption band is observed, centred at 3478.9.

By comparing the infrared absorption spectra of ZnO powders doped with 5% and 7% aluminium with those of undoped powders, we observe:

Strong absorption in the range 300 to 1000. In contrast to the spectrum of pure powders, the strong absorption attributed to ZnO, which was 429.123 in pure powders, is located at 438.78 in powders doped with 5% Al and at 440.744 in powders doped with 7% Al.

In aluminium-doped powders, new peaks appear at 560, 567, 669, 182, and at 497, 74, 565, 4, and 669. In powders doped with 5% and 7% aluminium, these peaks are close to those calculated for the spinel phase at 510, 562, and 667. After 1000, a low absorption band is observed with the same peaks in the pure powders [23, 24].

Table 8: Some important absorption bands of the IR spectrum.

Functional grouping	Experimental frequencies	Frequencies of literature
bond deformation vibration C =O	2356.31cm^{-1}	at 1560 cm^{-1}[25] et 1420 cm^{-1}[25]
elongation vibration of the bond O-H	3419 cm^{-1}	at ~ 3434 cm^{-1} [25] 3070-3850cm^{-1}[24]
The vibration of the bond Zn-O	429.123 $cm^{-1}$for ZnO pur 438.78 cm^{-1} for *Al-doped ZnO 5%* 440.744 cm^{-1} *of Al-doped ZnO 7%*	437.33cm^{-1} 460 cm^{-1} [25] 530-555cm^{-1} [24]
Spinel phase assigned $ZnAl_2O_4$	at 497.74cm^{-1} 565.39$cm^{-1}$and 669.18cm^{-1}	510,562cm^{-1},and 667cm^{-1}

4. Conclusions

This work detected the structural characterization of pure and aluminium-doped ZnO nanopowders and thin films using identification techniques such as X-ray diffraction, UV-visible, and infrared absorption spectroscopy. XRD analysis allowed us to observe the formation of hexagonal ZnO (wurtzite). There was a shift in the diffraction peaks of aluminium-doped ZnO compared to pure zinc oxide. This is attributed to the stresses applied to the nanopowder. We also observed a decrease in grain size due to increased doping, while the grain size increased under the influence of calcination temperature. UV-Visible analysis allowed us to calculate the energy gap (E_g) using the Tauc method, showing that the E_g value is approximately 4.12 eV. IR absorption spectroscopy appears to indicate the appearance of absorption peaks attributed to a spinel phase that does not appear in X-rays.

Conflict of interest

Authors declare that they have no conflict of interest.

References

1. J. A. Sans, A. Segura, M. Mollar, and B. Mar, Thin Solid Films, **453** , 251 (2004).
2. Y. Kashiwaba, F. Katahira, K. Haga, T. Sekiguchi, H. Watanabe, J. Crystal Growth, **221**, 431 (2000).
3. F. Paraguay, D. W. Estrada, L.D.R. Acosta, N.E. Andrade, and M. Miki-Yoshida, Thin Solid Films, **350**, 192 (1999).
4. M .N. Kamalasanan and S. Chandra, Thin Solid Films **288**, 112 (1996).
5. M. De la Olvera, A. Madonado, R. Asomoz, and M. Melendez-Lira, Sol. Energy Mater and Solar Cells, **41**, 61 (2002).
6. S. Kuo, W. Chen, F. Lai, C. Cheng, H. Kuo, S. Wang, and W. Hsieh, J. Cristal Growth **287**, 78 (2006).
7. H. Yang, J. S. Lee, S. Bae, and J. H Hwang, Current Applied Physics, **9**, 797 (2009).
8. U. Ozgur, Y. I. Alivov, C. Liu, A. Teke, M. A. Reshchikov, S. Dogan, V. Avrutin, S. J. Cho, and H. Morkoc, Journal of Applied Physics, **98**(4), 041301 (2005). DOI: 10.1063/1.1992666.
9. C. J. Brinker, G. C. Frye, A. J. Hurd, and C. S. Ashley, Thin Solid Films, **201,** 97 (1991).
10. A. Elkaiem, MSc thesis, University of Constantine, 2015.
11. G.A. Addle, Egypt J. Sol., **23(**2), (2000).
12. F. Melle Lakhdari, MSc thesis, University of sciences and technology of Mohamed Boudiaf Oran, 2008.
13. B. H. Nasir and M. I. Manssor, Rafidain Journal of Science, **23**, 163 (2012) DOI: 1033899/rjs.2012.59641
14. K. F. Konan, B. Hartiti, B. Aka, A. Ridah, K. Dakhsi, Y. Arba, and P. Thevenin, Afrique Science, **06**(1), 29 (2010).
15. Z. J. Shanan, S. M. Hadi, and S. K. Shanshool, Baghdad Sci. J., **15**, 0211 (2018). DOI: 10.21123/bsj.2018.15.2.0211.
16. S. Amara, and M. Bouafia, Int. J. Nanoparticles, **6**(2), (2013).
17. N. Talebian, M. R. Nilforoushan, and E. B. Zargar, Appl. Surf. Sci., **258**, 547 (2011). DOI: 10.1016/j.apsusc.2011.08.070.

18. F. Urbach, Phys. Rev. **92**, 1324 (1953).
19. H. Habieb and N. E. Hamdadou, Communication Science & technology **21**. (2019).
20. Z. M. Gibbs, A. LaLonde, and G. J. Snyder, New Journal of Physics, **15**, 075020 (2013). doi:10.1088/1367-2630/15/7/075020
21. J. C. Manifacier, J. Gasiot, and J. P. Fillard, J. Phys., E **9**, 1002 (1976). DOI:10.1088/0022-3735/9/11/032.
22. T. Srinivasulu, K. Saritha, and K. T. Ramakrishna Reddy, Modern Electronic Materials, **1779**, , S2452 (2017). DOI: http://dx.doi.org/10.1016/j.moem.2017.07.001.
23. E. R. Shaabana, I. S. Yahiab, and E. G. El-Metwally, Acta Physica Polonica A, **121**, (2012).
24. S. Ilican, M. Caglar, and Y. Caglar, Materials Science-Poland, **25** (3), (2007).
25. A. Chelouche, A. Aksas, D. Djoadi, J. Elghoul, L. Elmir, and S. Saoudi, in *International Conference on Laser and Applications, UKM Ouargla, 2009.*

المساهمة في تطوير المواد النانوية المركبة بناءً على دراسة هيكلية وبصرية لأكسيد الزنك وبولي مثيل ميثا اكريليت

القايم عبدالله[1] وبوكراع عمر[1]

[1] جامعة ورقلة، كلية الرياضيات وعلوم المواد، مخبر تطوير الطاقات الجديدة والمتجددة في المناطق القاحلة والصحراوية، ورقلة 30000، الجزائر

الخلاصة

تم إنشاء أغشية رقيقة من أوكسيد الزنك/بولي ميثيل ميثاكريلات (ZnO/PMMA) النقي والمُشَوَّب بالألمنيوم (Al) بكميتين مختلفتين (5% و7%) باستخدام طريقتي السول-جل والطلاء الدوراني، ثم سُخِّنت عند درجتي حرارة (450 و750 درجة مئوية). استُخدمت العديد من الخصائص لتحليل العينات الناتجة، بما في ذلك حيود الأشعة السينية (XRD)، والأشعة فوق البنفسجية المرئية، والأشعة تحت الحمراء (IR). أظهر تحليل حيود الأشعة السينية للعينات أنها شكلت بنية سداسية من ZnO تُعرف باسم wurtzite، باتجاه مفضل مُشار إليه بـ (101). ساعد تحليل الأشعة فوق البنفسجية المرئية للخصائص البصرية للعينات في حساب طاقة الفجوة باستخدام طريقة Tauc. تبلغ قيمة الطاقة 4.12 إلكترون فولت. تم تحليل الخصائص البصرية للعينات بواسطة جهاز تحويل فورييه بالأشعة تحت الحمراء (FTIR)، والذي أظهر وجود قمم امتصاص منسوبة إلى وجود الطور الجديد الذي لا يمكن ملاحظته من خلال الأشعة السينية وهو طور ألومينات الزنك السبينيل ($ZnAl_2O_4$).

الكلمات المفتاحيه: مسحوق نانوي، أغشية رقيقة من أوكسيد الزنك، هلام السول، سبينيل الطور، ألومينات الزنك السبينيل.